

Extracellular Subunit Interactions Control Transitions between Functional States of Acid-sensing Ion Channel 1a*

Received for publication, January 28, 2015, and in revised form, June 2, 2015. Published, JBC Papers in Press, June 12, 2015, DOI 10.1074/jbc.M115.641688

Karolina Gwiazda, Gaetano Bonifacio, Sabrina Vullo, and Stephan Kellenberger¹

From the Department of Pharmacology and Toxicology, University of Lausanne, Rue du Bugnon 27, CH-1005 Lausanne, Switzerland

Background: It is currently not known how extracellular interaction surfaces between ASIC subunits change during channel activity.

Results: Different engineered extracellular intersubunit disulfide bonds lock ASIC1a in open or non-conducting states.

Conclusion: Subunit interactions are critical for the ASIC gating process.

Significance: This study highlights new features of the mechanisms by which the pH controls ASIC activity.

Acid-sensing ion channels (ASICs) are neuronal, voltage-independent Na⁺ channels that are transiently activated by extracellular acidification. They are involved in pain sensation, the expression of fear, and in neurodegeneration after ischemic stroke. Our study investigates the role of extracellular subunit interactions in ASIC1a function. We identified two regions involved in critical intersubunit interactions. First, formation of an engineered disulfide bond between the palm and thumb domains leads to partial channel closure. Second, linking Glu-235 of a finger loop to either one of two different residues of the knuckle of a neighboring subunit opens the channel at physiological pH or disrupts its activity. This suggests that one finger-knuckle disulfide bond (E235C/K393C) sets the channel in an open state, whereas the other (E235C/Y389C) switches the channel to a non-conducting state. Voltage-clamp fluorometry experiments indicate that both the finger loop and the knuckle move away from the β -ball residue Trp-233 during acidification and subsequent desensitization. Together, these observations reveal that ASIC1a opening is accompanied by a distance increase between adjacent thumb and palm domains as well as a movement of Glu-235 relative to the knuckle helix. Our study identifies subunit interactions in the extracellular loop and shows that dynamic changes of these interactions are critical for normal ASIC function.

Acid-sensing ion channels (ASICs)² are neuronal acid-activated Na⁺ channels (1, 2) that belong to the epithelial sodium channel/degenerin family (3). ASICs contribute to the expression of fear (4), pain perception (2), and neurodegeneration after ischemia (5). Functional ASIC channels are formed by

three identical or homologous subunits (6, 7). So far eight ASIC isoforms have been described (2). Of these, ASIC1a is the most abundant subunit in the mammalian central nervous system (2). The closely related chicken ASIC1 (90% sequence identity with human ASIC1a; Fig. 1) has been crystallized in desensitized and toxin-opened conformations, providing important insights into the structural organization of ASICs (6, 8–11). Each ASIC subunit contains two transmembrane helices, short intracellular N and C termini and a large ectodomain with distinct subdomains, which are named palm, β -ball, knuckle, finger, and thumb (Fig. 2A). Changing the extracellular pH from the physiological 7.4 to acidic values opens and then desensitizes the ASICs, resulting in a transient current. Protonation of several residues per subunit in the extracellular domains finger, thumb, and palm contributes to ASIC activation (6, 12, 13).

The ASIC subunits interact with each other to form the channel trimer. ASICs undergo conformational changes during activity (14), which likely changes these intersubunit interactions. The fact that the inhibitory toxin Psalmotoxin 1 binds at subunit interfaces (9, 11) underlines the functional importance of subunit interactions. A recent study suggested that the dynamic formation of intersubunit disulfide bonds between intracellular C-terminal Cys residues may regulate ASIC activity as a function of the redox state (15). However, no molecular information is available on the interactions between extracellular domains of the ASIC subunits. In the present study we identified a palm-thumb and two finger loop-knuckle residue pairs predicted to form intersubunit hydrogen bonds. We show that engineered disulfide bonds between these residues impede channel opening in the case of the palm-thumb pair and promote either the open or a non-conducting state in the case of the two finger loop-knuckle pairs. These findings reveal unexpected roles of the geometries of the palm-thumb and knuckle-finger interactions in the control of the functional state of the ASIC pore.

Experimental Procedures

Molecular Biology—The human ASIC1a cDNA (16) was cloned into a vector containing 5'- and 3'-untranslated sequences of *Xenopus* β -globin. Wild type (WT) and mutants used in all experiments except voltage-clamp fluorometry

* This work was supported by Swiss National Science Foundation Grant 13003A_153419 (to S. K.). The authors declare that they have no conflicts of interest with the contents of this article.

¹ To whom correspondence should be addressed. Tel.: 4121-692-5422; Fax: 4121-692-5355; E-mail: Stephan.Kellenberger@unil.ch.

² The abbreviations used are: ASIC, acid-sensing ion channel; CuPhe, copper phenanthroline; ΔF , fluorescence change, $\Delta F/F$, relative fluorescence change; $I_{pH 6}$, current amplitude induced by pH 6; MBS, modified Barth's saline; pHDes₅₀, pH of half-maximal desensitization; pH₅₀, pH of half-maximal activation; SSD, steady-state desensitization; TCEP, Tris(2-carboxyethyl)phosphine hydrochloride; VCF, voltage-clamp fluorometry.

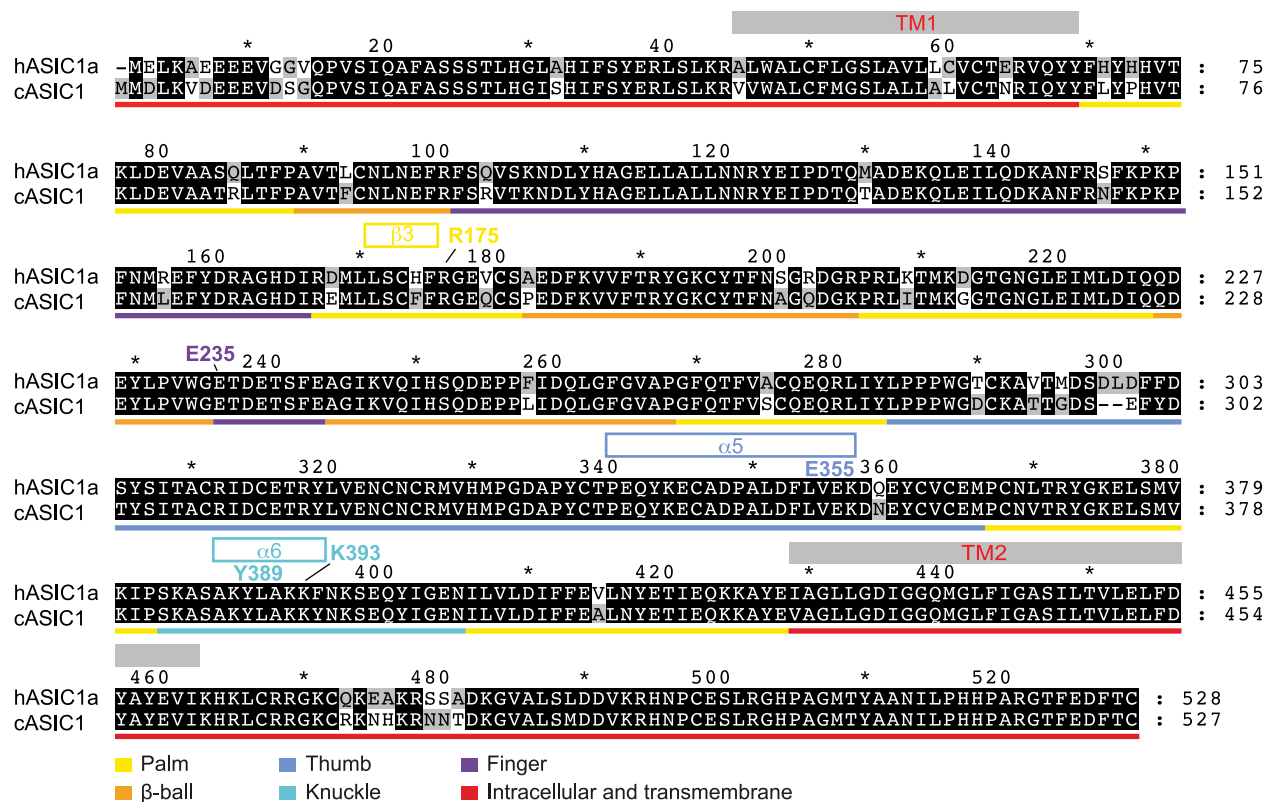


FIGURE 1. **Sequence alignment of human ASIC1a and chicken ASIC1.** The two protein sequences were aligned by using the ClustalX program. Identical residues are shown in white on a black background. The location of the transmembrane domains (TM1 and TM2) and structural elements in the vicinity of residues investigated in this study, the β sheet 3 of the palm, the α 5 helix of the thumb, and the α 6 helix of the knuckle are indicated above the sequence. In addition, the location of the residues of main interest in this study is shown. The colored line below the sequence identifies the different channel domains.

(VCF) experiments had a hemagglutinin (HA) tag inserted in the extracellular loop between residues Phe-147 and Lys-148 (17). Point mutations were introduced by QuikChange (Stratagene) and verified by sequencing (Syngene Biotech, Zurich). *In vitro* transcription was performed using the mMACHINE SP6 kit (Life Technologies, Zug, Switzerland).

Expression in *Xenopus* Oocytes—All experimental procedures on *Xenopus laevis* were carried out in accordance with the Swiss federal law on animal welfare and had been approved by the committee on animal experimentation of the Canton de Vaud. Oocytes from stage V and VI from female *X. laevis* were treated with collagenase, defolliculated, isolated as described previously (18), and injected with 50–100 nl of cRNA (0.4–0.6 μ g/ μ l for mutants and 0.03 μ g/ μ l for WT). The oocytes were kept in modified Barth's saline (MBS) composed of 85 mM NaCl, 1 mM KCl, 2.4 mM NaHCO₃, 0.33 mM Ca(NO₃)₂, 0.82 mM MgSO₄, 0.41 mM CaCl₂, 10 mM HEPES, 4.08 mM NaOH. Where indicated, oocytes were maintained in MBS containing 1 mM Tris(2-carboxyethyl)phosphine hydrochloride (TCEP) to prevent oxidation. Oocytes used for VCF experiments were incubated after RNA injection for 1 h with 10 mM 3-maleimidopropionic acid (Bachem) dissolved in MBS solution to modify the free Cys residues of proteins present on the oocyte surface.

Solutions and Reagents—Recording solutions contained 110 mM NaCl, 2 mM CaCl₂, and 10 mM HEPES (MES for pH \leq 6.8). 10 mM stock solutions of AlexaFluor 488 C-5 maleimide (Life Technologies, Zug, Switzerland) and CF 488A maleimide (Biotium, Basel, Switzerland) were prepared in DMSO.

All oxidation/reduction treatments except where explicitly indicated were done as follows. Oocytes were perfused with recording solution at physiological, pH 7.4, and ASICs were initially activated twice with an acidic pH at an interval of 1 min. Then the oxidative agent copper-*o*-phenanthroline complex (150 μ M CuSO₄, 450 μ M phenanthroline) was applied for 3 min followed by a 3-min application of recording solution supplemented with 5 mM EGTA and 2 mM MgCl₂ and a 2-min wash with normal recording solution, both at pH 7.4. The reducing agent TCEP was applied in electrophysiological experiments at 1 mM for 3 min followed by a 2-min wash with recording solution.

Measurement of Cell Surface Expression—cRNA (20 ng per oocyte) coding for WT ASIC1a and different simple and double cysteine mutants (carrying an extracellular HA tag as described above) was injected into *Xenopus* oocytes. 48 h after injection, the surface expression was measured as described (17). Briefly, mouse anti-HA antibody (clone HA-7; 0.5 μ g/ml; Sigma) and peroxidase-conjugated anti-mouse secondary antibody (2 μ g/ml; Amersham Biosciences) were used to label the surface-expressed HA-tagged ASIC1a constructs. Chemiluminescence of single oocytes was detected with a Victor 3 Multiwell Microplate Reader (PerkinElmer Life Sciences) using SuperSignal Elisa Femto Maximum Sensitivity Substrate (Thermo Scientific).

Electrophysiology and Voltage-clamp Fluorometry—Electrophysiological measurements were performed 1–3 days after cRNA injection. Currents were recorded with a Dagan TEV-

ASIC Subunit Interactions

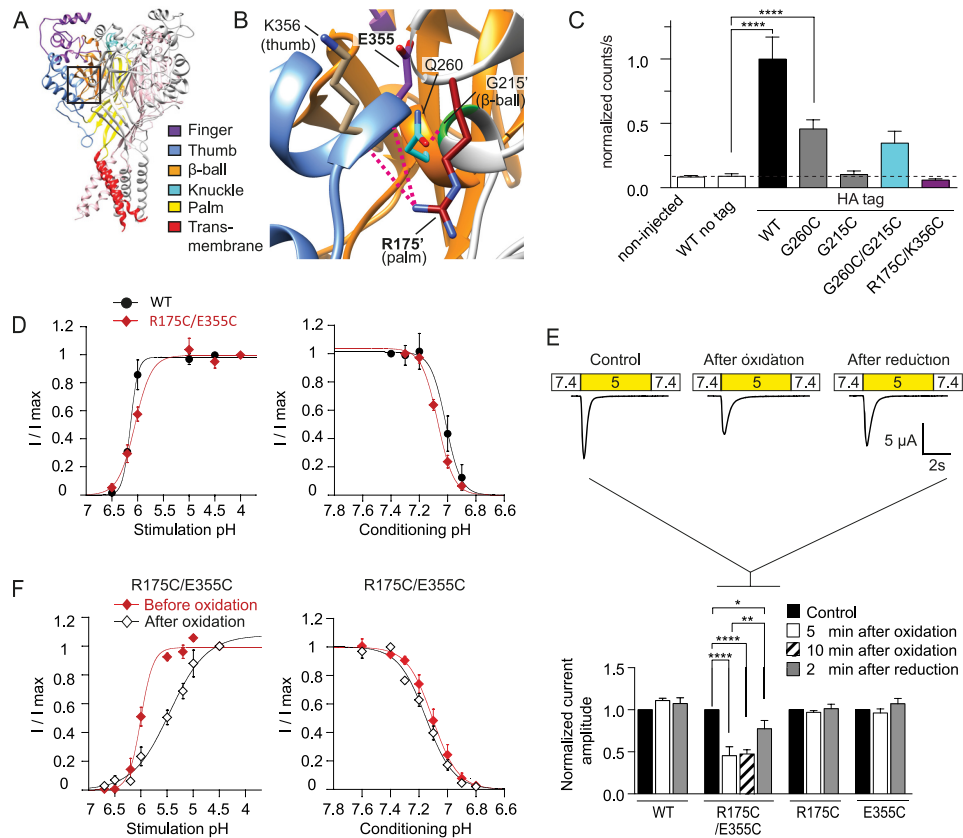


FIGURE 2. Interaction between Arg-175 and Glu-355 impedes ASIC opening. *A*, structural model of human ASIC1a, based on the crystal structure of chicken ASIC1 (10). Distinct domains of one subunit are indicated by different colors. The *black frame* indicates the location of the detailed view shown in *panel B*. *B*, view of predicted intersubunit interactions close to the acidic pocket. Predicted hydrogen bonds (Arg-175–Glu-355, Arg-175–Lys-356, and Gly-215–Gln-260) are shown as *pink dashed lines*. The distance between the nitrogen atom of the Arg-175 side chain and the oxygen atom of the Glu-355 backbone, predicted to form a hydrogen bond, is 3.4 Å. The corresponding distance was for both the Arg-175–Lys-356 and Gly-215–Gln-260 pair 2.8 Å. *C*, surface expression of HA-tagged ASIC1a was determined as described under “Experimental Procedures.” Untagged ASIC1a and non-injected oocytes (*open bars*) served as controls. Results are expressed as relative light units per second per oocyte, normalized at each experimental day to the average signal obtained with HA-tagged ASIC1a WT. The *dotted black line* represents the reference background signal corresponding to the untagged ASIC1a ($n = 36–52$; WT), $p < 0.0001$. *D*, activation curve plotting the normalized current response as a function of the stimulation pH (*left panel*, conditioning pH = 7.4) and SSD curve plotting the normalized current amplitude as a function of the conditioning pH (*right panel*, stimulation pH = 5). *red symbols*, ASIC1a R175C/E355C; *black*, WT. $n = 3–4$. The pH of half-maximal activation (pH_{50}) and desensitization ($pHDes_{50}$) values were obtained from fits to the experimental data. $pH_{50} = 6.06 \pm 0.05$ ($n = 4$; R175C/E355C) and 6.14 ± 0.02 ($n = 3$; WT); $pHDes_{50} = 7.07 \pm 0.01$ ($n = 4$; R175C/E355C) and 7.03 ± 0.01 ($n = 3$; WT). These values were not different between mutant and WT ($p > 0.05$). *E*, representative current traces of the R175C/E355C mutant during the oxidation/reduction treatment (*upper panel*). *Lower panel*, a *bar graph* representing pH 5-induced current amplitudes normalized to control before oxidation (*black bars*), after oxidation treatment with CuPhe and a 5-min wash (“Experimental Procedures,” *open bars*), or 10 min (*open, hatched bars*) and after subsequent reducing treatment with TCEP (*gray bars*, $n = 3–11$; see “Experimental Procedures”). *, $p < 0.05$; **, $p < 0.01$; ****, $p < 0.0001$, as compared with control. *F*, activation (*left*) and SSD (*right*) pH dependence of R175C/E355C before (*red symbols*) and after treatment with CuPhe (*open symbols*). Activation: conditioning pH = 7.4, pH_{50} , ctrl = 5.93 ± 0.05 , CuPhe = 5.43 ± 0.08 ; Hill coefficient (n_H), ctrl = 2.92 ± 0.25 , CuPhe = 1.32 ± 0.13 ; $p < 0.01$ (pH_{50}) and $p < 0.001$ (n_H), $n = 5–6$. SSD: stimulation pH = 5, $pHDes_{50}$, ctrl = 7.10 ± 0.03 , CuPhe = 7.16 ± 0.02 ; $p = 0.12$ $n = 9–10$.

200 amplifier (Minneapolis, MN) equipped with two bath electrodes at a holding potential of -60 mV (-40 mV in VCF experiments). Oocytes were placed in a recording chamber and perfused by gravity at a rate of 10–12 ml/min. To determine the activation and steady-state desensitization (SSD) pH dependence, oocytes were exposed for 55 s to the conditioning pH solution, and ASICs were activated every min by a 5-s acidification.

VCF measurements were carried out as described previously (14). Briefly, oocytes were labeled in the dark with 5 μ M AlexaFluor 488 C-5 maleimide or CF 488 maleimide at 19 °C for 15 min. The VCF setup was equipped with an Intensilight lamp (C-HGFI, Nikon). The signal emitted by the labeled oocyte was detected with a 40 \times oil-immersion objective (CFI Plan Fluor, Nikon) and measured by a photodiode (S1336–18BQ, Hamamatsu Photonics). Changes in fluorescence intensity (ΔF)

were normalized to the total fluorescence intensity (determined with a scalable offset device) as $\Delta F/F$. The signal was filtered and amplified by a low pass eight-pole Bessel filter (LPF-8, Warner Instruments) at 40 Hz. Each Cys mutant used for VCF was initially tested with each of the two fluorophores in two different protocols, acidification to pH 6 from a conditioning pH of either pH 7.4, at which the channels are closed and acidification produced a current (closed-open protocol), and from a conditioning pH at which the channels were desensitized (usually pH 6.7), where acidification did not induce a current (desensitized-open protocol). We considered fluorescence changes (ΔF) measured in the desensitized-open protocol as potential artifacts due to intrinsic pH dependence of the fluorophore in its specific environment (14) and used the fluorophore for which the ratio of the desensitized-open/closed-open $\Delta F/F$ was lower. AlexaFluor 488 was used for E235C and all

derived double mutants, whereas CF488A was used for K388C, Y389C, and K392C and all derived double mutants. Mutants in which the ratio of the desensitized-open/closed-open ΔF was >0.2 were not used for analysis. In the measuring chamber used to carry out the VCF experiments, fluorescence is measured on a surface of ~ 0.5 -mm diameter (corresponding to $\sim 20\%$ of the oocyte surface), whereas the current is measured on the entire oocyte surface. The kinetics of perfusion change in the VCF measuring chamber that we used for these experiments have previously been measured (14). This test showed that the delay in appearance of the new solution, caused by the dead volume of the system, was 685 ± 27 ms for the ΔF and 597 ± 24 ms for the current signal; thus there is a difference of <100 ms. The rise time of solution change was 346 ± 13 ms for the ΔF and 301 ± 19 ms for the current signal (14).

Ion selectivity of ASIC1a was investigated by recording the current-voltage relationship using either Na^+ - or K^+ -containing recording solutions (110 mM NaCl or 110 mM KCl, 2 mM MgCl_2 , 0.1 mM CaCl_2 , and 10 mM HEPES (or 10 mM MES for $\text{pH} \leq 6.8$)). The pH was adjusted using NaOH, except for solutions containing KCl, whose pH was adjusted with KOH. A ramp protocol was used to determine the reversal potential of the ASIC leak and peak current. From a holding potential of -60 mV, oocytes were held during 500 ms at -120 mV followed by a voltage ramp from -120 to $+60$ mV for the duration of 90 ms. This ramp protocol was run at pH 7.4 (baseline and leak current) and at the peak of the pH5-induced current to determine the peak current I-V relationship.

Data Analysis—Electrophysiological measurements on oocytes were recorded and analyzed using pClamp 9.2 (Molecular Devices, Sunnyvale, CA), or ChartMaster (HEKA, Lambrrecht, Germany; for VCF experiments). The pH of half-maximal activation (pH_{50}) was determined by fitting normalized activation curves to the Hill equation, $I = I_{\text{max}} / (1 + (10^{-\text{pH}50} / 10^{-\text{pH}})^{n_H})$, where I_{max} is the maximal current amplitude, pH_{50} is the value at which the current amplitude is half-maximal, and n_H is the Hill coefficient (Kaleidagraph 4.0, Synergy Software, Reading, PA). SSD curves were fitted by an analogous equation. Na^+/K^+ permeability ratios were calculated from the difference in reversal potential (E_{rev}) obtained in the presence of extracellular Na^+ or K^+ solution according to the equation $\Delta E_{\text{rev}} = E_{\text{rev, Na}} - E_{\text{rev, K}} = (RT/zF) \cdot \ln(P_{\text{Na}} \cdot [\text{Na}]_o / P_{\text{K}} \cdot [\text{K}]_o)$, where R is the gas constant, T is the temperature in K, z is the valence of the ion, F is the Faraday constant, P_{Na} and P_{K} are the relative permeabilities of Na^+ and K^+ , respectively, and $[\text{Na}]_o$ and $[\text{K}]_o$ are the extracellular concentrations of these ions (19).

Molecular graphics images were obtained using Chimera (20) from a homology model of human ASIC1a based on the crystal structure of chicken ASIC1 with PDB code 3HGC (10). A sequence alignment of human ASIC1a and chicken ASIC1 is shown in Fig. 1.

Statistics—Statistical analysis were performed using software Prism version 6.00 (GraphPad Software, La Jolla, CA). The distribution of the experimental population was verified with the Shapiro-Wilk normality test. For Gaussian distributions, parametric tests were performed (one-way analysis of variance followed by Tukey's multiple comparisons test or unpaired t test with Welch's correction for comparison of two conditions). For

distributions that were not Gaussian, non-parametric tests were used (Kruskal-Wallis followed by Dunn's multiple comparisons test or Mann-Whitney test for two conditions). All data are expressed as the mean \pm S.E. of independent experiments.

Results

We considered that residue pairs forming extracellular inter-subunit hydrogen bonds in ASIC1a likely participate in functionally important interactions between ASIC subunits. Analysis of an ASIC1a model based on the second published ASIC structure (10) using Chimera (20) predicted hydrogen bonds between the side chain of the palm residue Arg-175 and the backbone of two thumb residues, Glu-355 and Lys-356 and the β -ball domains of adjacent subunits (Gly-215 backbone-Gln-260 side chain; Fig. 2B) as well as between the finger loop of the β -ball and the knuckle (side chain-side chain; see Fig. 4A). Double Cys mutations between these pairs of residues were made in human ASIC1a (containing an HA tag in the finger domain (17)) to study the functional relevance of these interactions. Among them, combined mutations of the pairs G215C (β -ball)/Q260C (β -ball) and R175C (palm)/K356C (thumb) led to loss of current. We analyzed the cell surface expression of Cys double mutants by using an approach that consists of binding of a primary antibody to an extracellular HA tag on ASIC1a at the surface of intact oocytes. After binding of a horseradish peroxidase-conjugated secondary antibody and the addition of a substrate, chemiluminescence is measured on single, intact oocytes (21). Results are expressed as relative light units per second and normalized to the WT signal for presentation (Fig. 2C). The surface expression signal of oocytes expressing the HA-tagged ASIC1a WT and the mutant G260C was significantly higher than that of non-injected or non-tagged ASIC1a-expressing oocytes. In contrast, G215C and the double mutants R175C/K356C and G215C/Q260C did not show any significant increase in cell surface expression relative to the negative controls despite a tendency of higher values of the G215C/Q260C double mutant (Fig. 2C).

The Interaction between Arg-175 and Glu-355 Impedes Channel Opening—The residue Glu-355 is located at the lower end of the thumb helix $\alpha 5$, and Arg-175 is part of a palm loop adjacent to β strand $\beta 3$ (Fig. 2B). The "acidic pocket," to which Glu-355 belongs, has been implicated in ASIC activation (6, 22). The side chain of Arg-175 of the palm is predicted to form a hydrogen bond with the backbone of Glu-355 (Fig. 2B). When expressed in *Xenopus* oocytes, the R175C/E355C double mutant was functional and its pH dependence of activation and SSD (corresponding to the transition from the closed to the desensitized state) was not different from that of WT (Fig. 2D, $p = 0.4$ and $p = 0.06$, respectively, $n = 3-4$). To test whether the interaction between Arg-175 and Glu-355 affects ASIC function, oocytes expressing the mutant R175C/E355C were exposed to the oxidant copper phenanthroline (CuPhe, 3 min, pH 7.4) that promotes disulfide bond formation. Application of EGTA-containing and normal recording solutions followed the exposure to CuPhe to remove any free copper (see "Experimental Procedures"). Oxidation decreased the pH 5-induced peak current amplitude by $53 \pm 4\%$, $n = 11$ (Fig. 2E). This effect was

ASIC Subunit Interactions

not spontaneously reversible, as even after 10 min of washout the inhibition persisted (*hatched bar* in Fig. 2E). The current decrease of the R175C/E355C double mutant was partially reversed by exposure to the reducing agent TCEP (1 mM, 3 min; Fig. 2E). Together with the fact that no current decrease upon exposure to the oxidant was observed in WT ASIC1a and the single mutants, this strongly suggests that the observed current decrease is due to disulfide bond formation between R175C and E355C. The absence of effects in the controls is consistent with previous studies showing that the effects of redox reagents on WT ASIC1a currents are reversible (23–25). Analysis of pH-dependent gating showed that oxidation induced a marked acidic shift and a decrease in the steepness of the pH dependence of activation (Fig. 2F, $p < 0.004$, $n = 5–6$) but did not affect the pH dependence of SSD (Fig. 2F, $p = 0.18$, $n = 9–10$). The difference in the pH dependence of activation predicts a decrease of $\sim 18\%$ that of the peak current amplitude at pH 5 after oxidation, indicating that the oxidation reduces the pH 5-induced current by decreasing the maximal current amplitude and by shifting the pH dependence to more acidic values. The observed current decrease is, therefore, in part due to a changed equilibrium between the closed and the open state, suggesting that disulfide bond formation between R175C and E355C stabilizes the closed state. Accordingly, these data imply that most likely Arg-175 and Glu-355 move away from each other upon channel opening. It is also possible that the change in distance between Arg-175 and Glu-355 might occur at a step preceding channel opening and not in the open state itself.

Role of Charges in the Arg-175–Glu-355 Interaction—Because the two residues of this pair are of opposite charge, we hypothesized that electrostatic forces may contribute to their interaction. Therefore, we determined how neutralization and charge reversal mutations of the individual residues affected channel function, and we tested whether a double charge reversal could restore WT channel properties. The presence of other charged or polarized residues in the environment of Arg-175 and Glu-355, which may also contribute to electrostatic interactions, is shown in Fig. 3A. The neutralization mutation R175Q induced a small acidic shift, and the charge reversal R175E induced a larger acidic shift in the pH dependence of activation and SSD (Fig. 3B). In contrast, neutralization and charge reversal mutations of Glu-355 did not affect the pH dependence of activation ($p = 0.1$) and shifted the pH dependence of SSD to more alkaline values (Fig. 3C), consistent with previous studies (13). The double charge reversal mutant R175E/E355R showed strong acidic shifts of its pH dependence as compared with WT (Fig. 3D), similar to the shifts observed in the single R175E mutant, indicating that double charge reversal failed to restore WT properties.

Approaching the Knuckle Residue Lys-393 to Glu-235 of a Finger Loop Opens the Channel—The side chain of residue Glu-235 of the finger loop originating in the β -ball was predicted to form hydrogen bonds with side chains of residues Tyr-389 and Lys-393 of the knuckle of a neighboring subunit (Fig. 4A). This finger loop points into the acidic pocket from the upper end of the palm, whereas the knuckle is located on the top of the palm. The E235C/K393C double mutation did not affect the pH

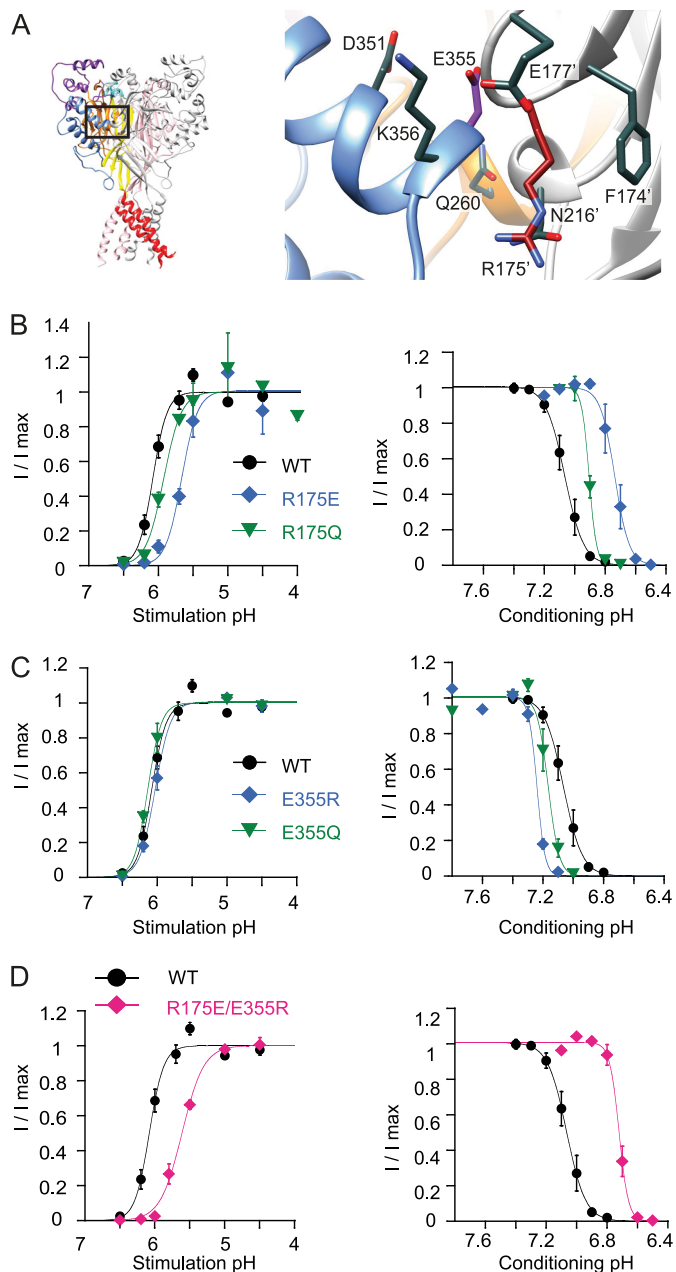


FIGURE 3. Role of electrostatic forces in the Arg-175–Glu-355 interaction. A, view of Arg-175, Glu-355, and neighboring residues (*side chains are in dark gray*). B–D, activation (*left panels*, conditioning pH = 7.4) and SSD (*right panels*, stimulation pH = 5) curves of mutants and WT. Fit parameters for WT were: activation $pH_{50} = 6.09 \pm 0.03$; $n = 9$; SSD, $pH_{Des50} = 7.06 \pm 0.02$, $n = 10$. B, Arg-175 charge reversal and neutralization mutants. pH_{50} : R175Q = 5.87 ± 0.05 , R175E = 5.67 ± 0.03 ; $n = 5–6$; WT versus R175E, $p < 0.001$; WT versus R175Q, $p > 0.05$. pH_{Des50} : R175Q = 6.90 ± 0.01 , R175E = 6.74 ± 0.03 ; $n = 6–8$; WT versus R175E, $p < 0.0001$; WT versus R175Q, $p > 0.05$. C, Glu-355 charge reversal and neutralization mutants. pH_{50} : E355Q = 6.13 ± 0.03 , E355R = 6.02 ± 0.03 ; $n = 4$; WT versus E355Q and E355R, $p = 0.1$. pH_{Des50} : E355Q = 7.17 ± 0.01 , E355R = 7.25 ± 0.003 ; $n = 3–4$; WT versus E355R, $p < 0.01$, WT versus E355Q, $p > 0.05$. D, double charge reversal mutation R175E/E355R. pH_{50} : 5.55 ± 0.06 ; $n = 5$; different from WT, $p < 0.001$. pH_{Des50} : 6.73 ± 0.02 ; $n = 4$; different from WT, $p < 0.002$.

dependence of activation (Fig. 4B). Interestingly, oocytes expressing this double mutant showed a significantly increased leak current at pH 7.4 compared with various controls (Fig. 4, C and D), suggesting that disulfide bond formation between E235C and K393C opens the channel. If oocytes injected with

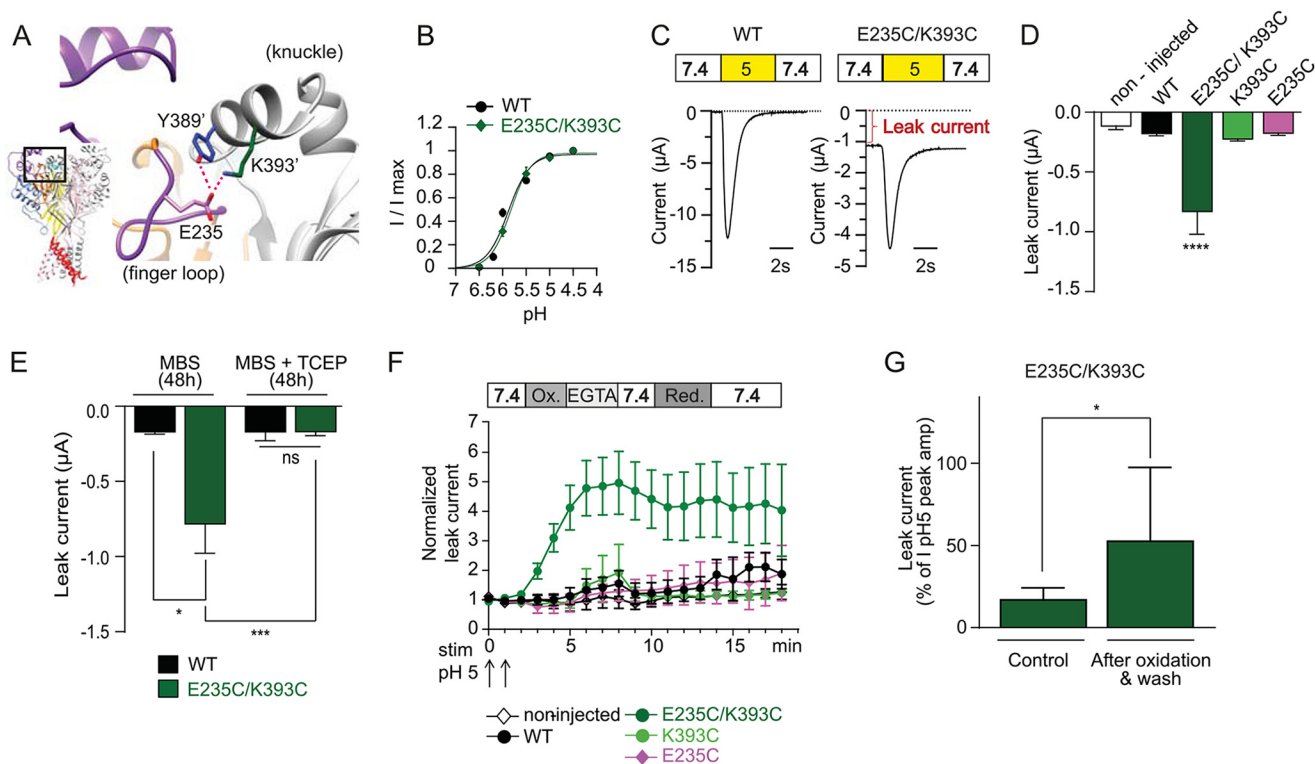


FIGURE 4. Interaction between Glu-235 and Lys-393 opens the channel. *A*, close-up view showing predicted hydrogen bonds (pink lines) between Glu-235 and the knuckle residues Lys-393 and Tyr-389. The distances between the atoms involved in the predicted hydrogen bonds, measured in the ASIC1a homology model, are 3.3 Å (Glu-235–Tyr-389) and 2.8 Å (Glu-235–Lys-393). *B*, activation pH dependence of E235C/K393C (green symbols) and WT (black); $n = 3-4$; $p = 0.8$. *C*, representative current traces of WT and E235C/K393C. *D*, leak current amplitudes at pH 7.4 of E235C/K393C and controls as indicated, without the addition of oxidation reagents; $n = 3-24$. The leak current amplitude of E235C/K393C is greater than that of other conditions (****, $p < 0.0001$). *E*, leak current of WT and E235C/K393C measured after incubation during the expression phase in normal MBS or MBS containing 1 mM TCEP; $n = 3-24$. *, $p < 0.05$; ***, $p < 0.001$. *ns*, not significant. *F*, evolution of the leak current under oxidation/reduction treatments as indicated. Ox. = Cu/Phe, Red. = 1 mM TCEP (see “Experimental Procedures”). Amplitudes are normalized to the average pH 7.4 current amplitude measured at 0 and 1 min. Arrows indicate the time points at which the pH 5-induced peak current amplitude was measured; $n = 3-10$. *G*, leak current of the E235C/K393C mutant measured at pH 7.4, before (control = mean of current amplitudes measured at 0 and 1 min in *F*) and after oxidation (mean of current amplitudes measured at 10 and 11 min in *F*), represented as the percentage of the pH 5-induced control peak current amplitude, $n = 10$; *, $p = 0.015$.

RNA coding for the E235C/K393C double mutant were kept during the expression phase in a solution containing the reducing agent TCEP (1 mM), they showed a normal leak current (Fig. 4*E*), further corroborating this conclusion. Incubation with TCEP did not affect the leak current observed with ASIC1a WT (Fig. 4*E*) nor did it change the pH_{50} of activation ($pH_{50} = 5.96 \pm 0.04$ (control) and 5.86 ± 0.08 (TCEP), $n = 6-7$). Exposure to CuPhe induced a significant increase in leak current in the double mutant but not in the controls (Fig. 4, *F* and *G*). The maximal amplitude of the CuPhe-induced leak current of the E235C/K393C mutant was variable, reaching on average ~50% of the pH 5-induced current amplitude (Fig. 4*G*). Very similar results were obtained when a different oxidant, H_2O_2 , was used instead of CuPhe, as indicated by the increase of the leak current after a 3-min exposure to 0.3% H_2O_2 (and subsequent wash) by 0.8 ± 0.1 -fold (WT; $n = 5$) and 3.0 ± 0.9 -fold (E235C/K393C; $n = 7$, $p = 0.003$). The absolute leak current amplitude of the E235C/K393C mutant after CuPhe treatment was $2.3 \pm 0.3 \mu A$ ($n = 19$) compared with $<0.4 \mu A$ in all other conditions. Exposure to TCEP did not reverse the effect of oxidation (Fig. 4*F*).

To compare the properties of the leak- and acid-induced peak currents of this double mutant, we determined their Na^+/K^+ selectivity and inhibition by amiloride. Voltage ramps

obtained with either extracellular Na^+ or K^+ showed the expected Na^+ over K^+ selectivity of the pH 5-induced E235C/K393C peak current (Fig. 5*A*). In contrast, the leak current was not Na^+/K^+ -selective (Fig. 5*B*). The Na^+/K^+ permeability ratio calculated from the difference in reversal potential determined in Na^+ - or K^+ -containing extracellular medium (see “Experimental Procedures”) was 4.9 ± 0.3 ($n = 5$, acid-induced current) and 1.0 ± 0.2 ($n = 5$, leak current, $p < 0.01$). Interestingly, previous studies showed evidence for similar changes in selectivity between the transient and sustained current of ASICs (9, 26). Amiloride is an established pore blocker of the epithelial Na^+ channel (27) and has also been shown to bind into the ASIC pore (28, 29). The E235C/K393C peak current showed lower affinity for inhibition by amiloride than the WT current (Fig. 5*C*). This is quite surprising given the fact that the two mutations are distant from the pore. Amiloride inhibited the leak current even at millimolar concentrations only partially (Fig. 5*C*). The difference in ion selectivity and amiloride inhibition compared with the peak current suggests that the pore conformation mediating the leak current may be somewhat different from the H^+ -induced open conformation. The leak current was pH-independent in the pH range 8–5 (Fig. 5*D*), indicating that the E235C-K393C interaction shortcuts pH-dependent ASIC activation.

ASIC Subunit Interactions

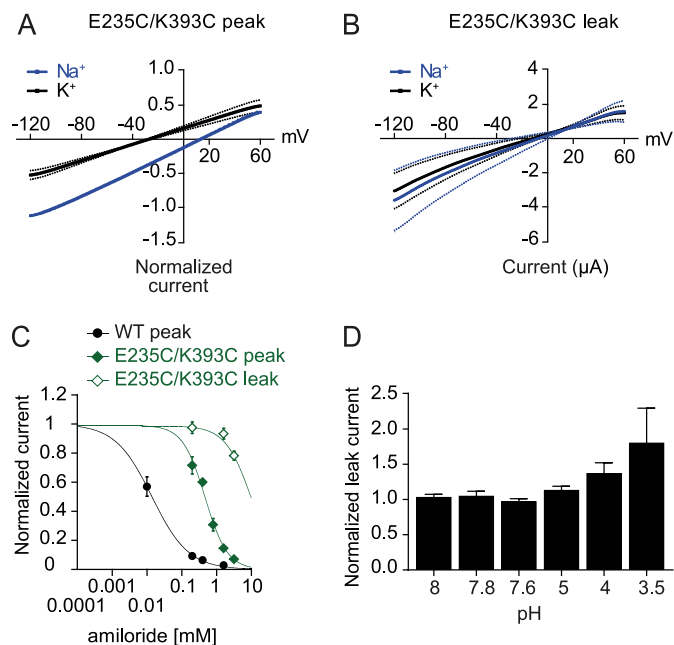


FIGURE 5. Permeability and inhibition by amiloride of E235C/K393C. *A*, a ramp protocol of 90 ms (−120 to +60 mV) was used to measure the permeability of the pH 5-induced peak current of E235C/K393C (see “Experimental Procedures”). The acid-induced current was determined as the difference between the ramp currents measured at pH 5 (during the peak) and at pH 7.4. For each cell, the acid-induced currents with extracellular Na⁺ and K⁺ solution were normalized to the amplitude measured with Na⁺ at −100 mV. Dotted lines represent the S.E. of independent experiments ($n = 5$). *B*, the same ramp protocol was used to determine the selectivity of the leak current ($n = 5$). The mean leak current amplitudes of non-injected oocytes ($n = 5$) were subtracted from individual measurements in the E235C/K393C mutant; dotted lines represent the S.E. of independent experiments. *C*, normalized peak (pH 5-induced) and leak current (pH 7.4) as a function of amiloride concentration. IC₅₀ values obtained from fits to the data were $19 \pm 9 \mu\text{M}$ (WT peak current), $0.41 \pm 0.06 \text{ mM}$ (E235C/K393C, peak current), and $9.4 \pm 1.9 \text{ mM}$ (E235C/K393C, leak current). *D*, pH dependence of E235C/K393C leak current. The pH of the extracellular solution was switched from 7.4 to the indicated values, and the average current amplitude was measured between 20 and 30 s after the solution change. These current amplitudes were normalized to the current measured at pH 7.4 before the solution change; $n = 4-6$. Changes to acidic pH induced a transient current that desensitized, however, within the first 20 s.

Interaction of E235C with Y389C Promotes a Non-conducting State—Because Glu-235 is predicted to form also a hydrogen bond with another knuckle residue, Tyr-389 (Fig. 4A), we measured the properties of the E235C/Y389C double mutant. When kept in normal MBS solution during the expression phase, the E235C/Y389C double mutant did not produce any transient current (Fig. 6A). However, if oocytes expressing this double mutant were incubated in MBS containing 1 mM TCEP during the expression phase, a pH 3-induced current of $1.51 \pm 0.17 \mu\text{A}$ ($n = 15$) was measured, strongly suggesting that the formation of a disulfide bond between E235C and Y389C prevented ASIC opening (Fig. 6A). This double mutation shifted the pH dependence of activation by ≥ 3 units to more acidic values (Fig. 6B, left panel). This shift in pH dependence is due to the simultaneous presence of Cys at the position of both, Glu-235 and Tyr-389, as the individual E235C mutation did not change the pH₅₀ (13), and the Y389C mutation induced an acidic shift of only ~ 0.5 units (Fig. 6B). The acidic shift of the SSD pH dependence of E235C/Y389C was comparatively small (Fig. 6B, right panel). When the E235C/Y389C channels were

exposed to CuPhe, the pH3-induced current disappeared almost completely and was only partially recovered by exposure to TCEP (Fig. 6C). Experiments aiming at uncovering a state dependence of disulfide bond formation, applying CuPhe under conditions in which channels were either closed or desensitized, showed no difference between the incubation conditions (data not shown). It is, therefore, difficult to establish whether disulfide bond formation between E235C and Y389C puts the channel rather in the closed or the desensitized state.

Mutation of Tyr-389 to different hydrophilic residues induced smaller shifts in pH dependence of activation than the one observed in the Cys double mutant and similar shifts in the pH dependence of SSD (Fig. 6, B and D). The mutation Y389K shifted the activation pH dependence to the largest extent. The long side chain of the Lys residue might distort the existing conformation of the finger loop-knuckle interface the most. Its positive charge likely attracts the Glu-235 side chain, thereby approaching the finger loop to the knuckle, which would reduce channel open probability, as does E235C-Y389C disulfide bond formation.

Movements of the β -Ball and the Knuckle during ASIC Activity—To obtain additional information on possible conformational changes of the knuckle and the finger loop, we applied VCF, which uses simultaneous electrophysiological and fluorescence measurements to correlate channel function with conformational changes in the immediate environment of a placed fluorophore. Observed fluorescence changes (ΔF) reflect changes in the environment of the fluorophore and in some cases depend on the proximity of a Trp residue that quenches the fluorescence signal (30). ASIC1a contains only one Trp residue in the proximity of the knuckle, Trp-233 of the β -ball (Fig. 7A). The Trp-233 residue sits on top of the finger loop that points into the acidic pocket and contains Glu-235. When the dye CF488A was attached to an engineered Cys residue at position Y389C, an increase in fluorescence was observed upon channel activation (Fig. 7, A and B). Similar fluorescence changes have been observed with the knuckle residues K388C and K392C and with residue E235C (Ref. 14 and Fig. 7A, by using the fluorophores CF488A with K388C and K392C and AlexaFluor 488 with E235C; see “Experimental Procedures”). To obtain information on the direction of these movements, we replaced Trp-233 by Val (which is not a fluorescence quencher) in these mutant channels. The current properties of these double mutant channels were similar to the single Cys mutants. The amplitude of the relative fluorescence change ($\Delta F/F$) divided by the current amplitude at pH 6 to normalize for channel expression ($\Delta F/F/I_{\text{pH } 6}$) was, however, dramatically decreased, indicating that the ΔF in the single mutants was mainly due to the presence of Trp-233 (Fig. 6, C and D). Because Trp-233 quenches the fluorescence signal, the positive ΔF observed upon channel activation (Fig. 7B and Ref. 14) indicates that the fluorophore attached to different knuckle and finger loop residues moves away from Trp-233. To further confirm that the loss of ΔF in the double mutants with W233V is due to the absence of quenching by Trp-233 and is thus specific to Trp-233, we combined each of the four Cys mutations, E235C, K388C, Y389C, and K392C, with mutations of other residues

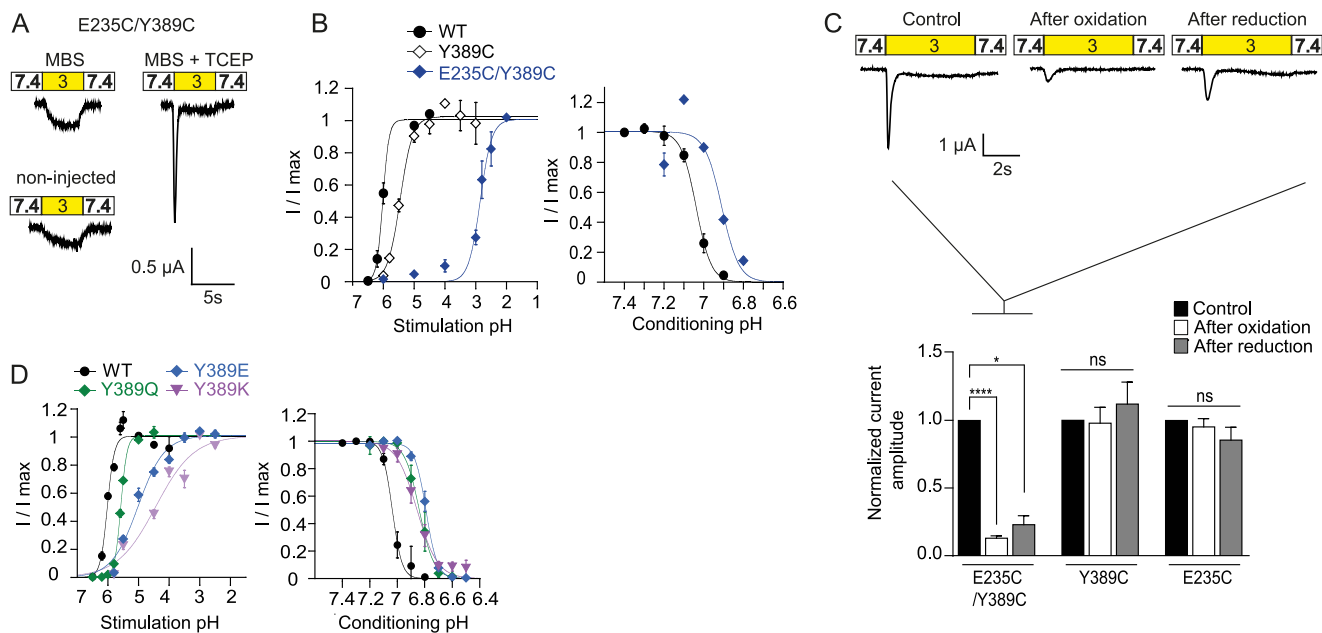


FIGURE 6. Interaction of E235C with Y389C prevents ASIC opening. **A**, current traces from an E235C/Y389C-expressing oocyte maintained during the expression phase in MBS or MBS supplemented with 1 mM TCEP and a non-injected oocyte as indicated. **B**, activation (left) and SSD (right) pH dependence of WT (black symbols), Y389C (open symbols), and E235C/Y389C (blue). pH_{50} values were 6.14 ± 0.04 (WT), 5.43 ± 0.05 (Y389C), and 2.79 ± 0.08 (E235C/Y389C) as determined from fits to the data ($n = 4-8$; WT versus Y389C, $p > 0.05$; WT versus E235C/Y389C, $p < 0.001$). pH_{Des50} values were 7.04 ± 0.01 (WT) and 6.91 ± 0.01 (E235C/Y389C); $n = 3-6$; WT versus E235C/Y389C, $p = 0.02$. **C**, representative current traces of E235C/Y389C at different stages of the oxidation/reduction treatment (upper panel). Lower panel, bar graph representing normalized current amplitudes before oxidation (black bars), after CuPhe treatment (open bars), and after subsequent reducing treatment with TCEP (gray bars, see "Experimental Procedures"); $n = 3-16$; *, $p < 0.05$, ****, $p < 0.0001$; ns, no significant difference to control. **D**, activation (conditioning pH = 7.4) and SSD pH dependence of WT, Y389E, Y389Q, and Y389K (stimulation pH = 5). pH_{50} values were 6.03 ± 0.01 (WT), 5.05 ± 0.08 (Y389E), 4.42 ± 0.12 (Y389Q), and 5.58 ± 0.01 (Y389K); $n = 5-9$; WT versus Y389Q, $p > 0.05$; WT versus Y389E, $p < 0.001$; WT versus Y389K, $p < 0.0001$. pH_{Des50} values were 7.04 ± 0.01 (WT), 6.79 ± 0.01 (Y389E), 6.86 ± 0.02 (Y389Q), and 6.84 ± 0.01 (Y389K); $n = 5-6$, WT versus Y389Q, $p < 0.05$; WT versus Y389E, $p < 0.001$; WT versus Y389K, $p > 0.05$.

located in close proximity whose positions are shown in Fig. 7E. All of these double mutants showed a positive ΔF upon extracellular acidification, as the single Cys mutants. In none of these double mutants was the $\Delta F/F_{pH6}$ smaller than in the corresponding single Cys mutant (Fig. 7F). The absence of significant decreases in $\Delta F/F_{pH6}$ in these control double mutants confirms the essential role of Trp-233 for the fluorescence signal in the four Cys mutants. In one of the double mutants, Y389C/E238C, the pH dependence of the current was substantially shifted to more acidic values as compared with the single mutant ($pH_{50} = 6.06 \pm 0.02$ (Y389C) and 5.64 ± 0.04 (Y389C/E238C), $n = 4-7$). In this double mutant, the pH 6-induced current amplitude amounted to $\sim 10\%$ of the maximal current amplitude induced by more acidic pH, whereas the corresponding amplitude was $>50\%$ in the single mutant. As a consequence of the low I_{pH6} , the $\Delta F/F_{pH6}$ ratio of this double mutant was much higher than that of the corresponding single mutant. This is, however, only due to the shift in pH dependence and does not reflect an increased $\Delta F/F$ per channel expressed at the cell surface. The pH_{50} values of other control double mutants were similar to the values of the corresponding single mutants (see the legend to Fig. 7F). In the K393C mutant channel, activation did not induce any change in fluorescence. The Lys-393 residue might be shielded from Trp-233 by other amino acid residues.

The ΔF of the knuckle residues K388C, K392C (previously shown (14)), and Y389C (Fig. 7, G and H) had fast kinetics. Fig. 7G compares the kinetics of the ΔF onset and of the current

appearance of Y389C, both measured as rise time, the time to pass from 10 to 90% of the maximal amplitude. The ΔF kinetics appear to be slightly slower, although the limited speed of solution change, which does not sufficiently resolve the kinetics of current appearance ("Experimental Procedures"), does not allow us to conclude whether this is indeed the case. The comparison of the kinetics of the ΔF onset and current decay (Fig. 7H) shows that ΔF onset is faster than current desensitization ($p < 0.01$). In our previous study we show that the kinetics of the E235C ΔF match the kinetics of current desensitization (14). This indicates that the movement of the knuckle occurs before the conformational changes in the finger loop. These observations complement the double Cys mutation experiments, which suggest that the conformational change leading to channel opening brings Glu-235 close to K393C.

Discussion

In the present study we identify subunit interactions in the ASIC1a ectodomain that are critical for channel function. A close interaction between the palm residue Arg-175 and Glu-355 of the thumb inhibits ASIC currents. Disulfide bond formation of E235C of a finger loop with two different knuckle residues can lock the channel either in an open (K393C) or a non-conductive state (Y389C), showing that the position of this finger loop relative to the knuckle acts like a switch on channel function.

Conformational Changes at the Thumb-Palm Interface—It has been suggested that during ASIC activation, protonation of

ASIC Subunit Interactions

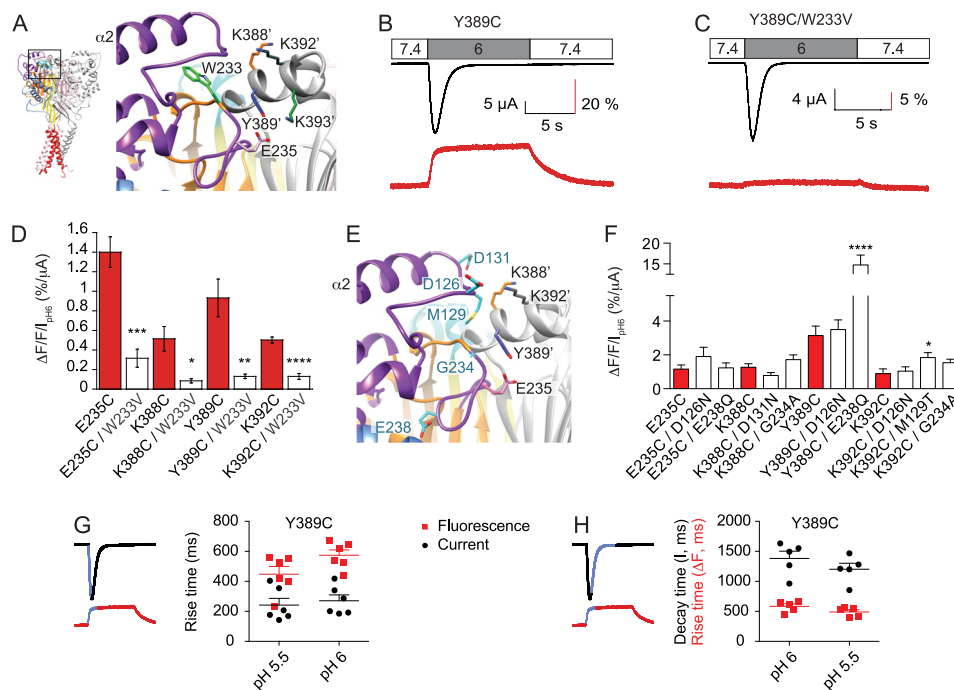


FIGURE 7. Distance increase between the knuckle and the β -ball upon acidification. *A*, structural model of ASIC1a based on the crystal structure of cASIC1 (10) and close-up showing the residues mutated for VCF in the knuckle, the finger, and the β -ball. *B* and *C*, representative current (black) and fluorescence change (ΔF) traces (red) of the single mutant Y389C and the double mutant Y389C/W233V. The vertical bars indicate the current amplitude (black), and $\Delta F/F$ is in % (red). *D*, relative fluorescence changes $\Delta F/F$ normalized to the pH 6-induced current amplitude, shown for E235C, K388C, Y389C, and K392C, and for each of these mutations combined with the W233V mutation; $n = 4-7$; *, $p < 0.05$, **, $p < 0.01$; ***, $p < 0.001$, ****, $p < 0.0001$ (different between single and corresponding double mutant). *E* and *F*, control experiments in which residues other than Trp-233 in the proximity of this residue were combined with the Cys mutants to test whether other mutations may also decrease the ΔF amplitude. The control mutations are shown in the structural model in *E*, with Gly-234 represented by an asterisk (*). *F*, $\Delta F/F_{pH6}$ values shown for E235C, K388C, Y389C, and K392C and for each of these mutations combined with other mutations in the proximity; $n = 6-8$. The increase in $\Delta F/F_{pH6}$ of the mutant Y389C/E238Q relative to the single mutant Y389C was due to an acidic shift of the activation pH dependence in the double mutant and not because of a higher $\Delta F/F$ per channel expressed at the cell surface. pH_{50} values of single and control double mutants were 6.41 ± 0.02 (E235C), 6.19 ± 0.06 (E235C/D126N), 6.17 ± 0.05 (E235C/E238Q), 6.31 ± 0.06 (K388C), 6.24 ± 0.02 (K388C/D131N), 6.20 ± 0.02 (K388C/G234A), 6.06 ± 0.02 (Y389C), 6.01 ± 0.03 (Y389C/D126N), 5.64 ± 0.04 (Y389C/E238Q), 6.27 ± 0.06 (K392C), 6.38 ± 0.01 (K392C/D126N), 6.29 ± 0.05 (K392C/M129T) and 6.25 ± 0.06 (K392C/G234A); $n = 4-7$. *G* and *H*, current and ΔF kinetics of the Y389C mutant. *G*, scatter plot showing the kinetics of the ΔF (red symbols) and current onset (black), as illustrated in the schematic view on the left by the blue parts of the traces. Kinetics are shown as rise time, the time to pass from 10 to 90% of the maximal amplitude. They were measured at both pH 5.5 and 6; $n = 6$. Due to the solution exchange time of ~ 300 ms ("Experimental Procedures") the current appearance kinetics are not properly resolved. *H*, the ΔF onset rise time (red) and current decay time (black) are compared in the scatter plot ($n = 5$; $p < 0.01$), as illustrated in the schematic view on the left by the blue parts of the traces.

Glu and Asp residues in the acidic pocket allows a movement that brings the finger, thumb, and β -ball closer to each other and that this movement induces channel opening and subsequent desensitization (6). Mutagenesis studies have indeed shown that residues of the acidic pocket together with protonatable residues in other domains such as, for example the palm, co-determine the pH dependence of ASICs (6, 12, 13, 31, 32). So far the only experimental indication for conformational changes in the acidic pocket comes from an observation by VCF suggesting that E355C moves during desensitization to a less exposed position, consistent with a closing of the acidic pocket (14). We show here that oxidative treatment of the E355C/R175C mutant leads to current inhibition. The fact that this inhibition is not spontaneously reversible but can be partially reversed by reducing agents and that it is observed in the double but not in the corresponding single mutants strongly suggests that it is due to disulfide bond formation between E355C and R175C. The inhibition is in part due to an acidic shift of the pH dependence of activation. That oxidation did not affect the SSD pH dependence suggests that the disulfide bond formation predominantly stabilizes the closed relative to the open state and, thus, that less mutant channels open upon acidification. There-

fore, Glu-355 and Arg-175 likely move away from each other during activation or a step preceding activation. Such a movement might be necessary for the closing of the acidic pocket.

One aspect of our observations regarding the Glu-355-Arg-175 interaction is difficult to understand. The functional analysis of combined charge reversal mutations of these two residues showed that the effects of the R175E mutation are dominant over those of the E355R mutation and that double charge reversal did not reconstitute WT properties. This behavior is compatible with a situation in which, as in the crystal structure, these two side chains point in different directions. Other electrostatic interactions between the $\alpha 5$ thumb helix and the palm loop that carries Arg-175, as for example between Glu-177 and Lys-356 (Fig. 3A), may be more important than the electrostatic interaction between these two residues. To allow formation of a disulfide bond between R175C and E355C upon oxidant exposure, the engineered residue Cys-355 has to completely change its orientation from the one shown in the crystal structure. The ASIC1a model used here is based on a crystal structure that likely represents the desensitized conformation (10). The orientation of the Arg-175 and Glu-355 side chains in the open ASIC structures is not different (8, 9), and their orien-

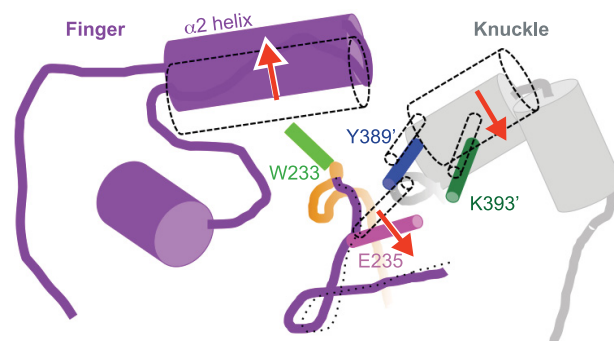


FIGURE 8. Model of intersubunit conformation changes in the finger loop-knuckle region. A knuckle (gray) and part of the finger (purple) and β -ball (orange) of a neighboring subunit in the open conformation are shown in a schematic. The hypothesized positions of some of these structural elements in the closed conformation are shown as dotted outlines. Red arrows indicate the conformational changes suggested to occur upon acidification. These conformational changes increase the distance between Trp-233 and the finger α 2 helix and the knuckle and bring Glu-235 away from Tyr-389, closer to Lys-393.

and Trp-233 move away from each other and that the ΔF is not just due to a rotation of the knuckle helix. Currently it is not known whether this conformational change occurs during opening or desensitization. Besides the rapid kinetics of the ΔF of labeled knuckle mutations, two observations suggest that the knuckle-finger loop interaction affects rather the closed-open than any desensitization-related functional transitions. First, the E235C/Y389C mutation affects activation much more than desensitization (Fig. 6B). Second, the position of Glu-235 relative to the knuckle is the same in crystal ASIC structures representing the open and the desensitized state, with the Glu-235 side chain located between Tyr-389 and Lys-393 (9, 10). The conformational changes in the finger and the knuckle documented by VCF represent, therefore, most likely transitions from a different functional state; thus from the closed channel conformation.

Based on our data obtained with the engineered Cys pairs and with VCF, we hypothesize that upon acidification the finger α 2 helix and the knuckle move away from Trp-233 of the β -ball and that the finger loop containing Glu-235 undergoes a change in conformation that brings the Glu-235 side chain from a position close to Tyr-389 to the proximity of Lys-393, as illustrated in Fig. 8. The difference in the relative orientation of Glu-235 and the knuckle might be small but sufficient to impose functional changes on the channel pore either via the knuckle and palm along the central axis of the channel or externally via the finger and the thumb.

Conclusion—In summary, our study demonstrates that the approach of a thumb residue to the neighboring palm tends to keep the channel in the closed conformation. The position of a finger loop residue relative to the neighboring knuckle switches the channel between an open and a non-conducting conformation. These observations show that protonation-dependent conformational changes within the individual subunits affect the interactions between subunits and the overall arrangement of the channel. These changes in subunit interactions are required for normal channel gating. The identified subunit interaction surfaces may be interesting target sites for novel ASIC drugs.

tation in the closed channel is not known. The side chain orientation of these residues before oxidation is most likely not different in the R175C/E355C double mutant from the one in WT, as the double Cys mutation did not change the current properties. It also seems unlikely that the side chain orientation of Arg-175 and Glu-355 might be different in human ASIC1a from the crystal structures obtained from chicken ASIC1 as the two ASIC subtypes show a high sequence homology (90%), the α 5 helix is completely conserved, and the palm loop containing Arg-175 is highly conserved and stabilized by a conserved disulfide bond between Cys-172 and Cys-179. Together, these observations suggest that the E355C side chain changes its orientation upon oxidation, and this conformational change may correspond to a movement undergone during channel closing.

Finger Loop-Knuckle Interactions Control ASIC Activity—Because the knuckle adopts the same conformation in crystal structures of the open and the desensitized state, it was concluded that it forms a rigid scaffold (9). However, VCF measurements detected rapid fluorescence changes in the knuckle, indicating that the knuckle itself or neighboring domains move during the transition from the closed to the open and desensitized states (14). Here, we first show that disulfide bond formation between E235C, located in the finger loop originating in the β -ball, and two different residues of the knuckle either promoted or prevented channel opening. Individual mutations of Glu-235 and Tyr-389 to Cys produced channels with normal current amplitudes and induced no, or only subtle, changes in pH dependence. In contrast, the double mutant E235C/Y389C was only functional if the oocytes were kept in a medium containing TCEP during the expression phase. In this condition the pH dependence of activation of the double mutant was strongly shifted toward more acidic values. This shift is, therefore, due to the simultaneous presence of Cys residues at positions 235 and 389. The strong shift of the pH_{50} in the E235C/Y389C double mutant but not in the corresponding single mutants and the current suppression by oxidation suggest that disulfide bond formation between E235C and Y389C at one or two subunit interfaces induces the observed shift in pH dependence, whereas the presence of disulfide bonds at two or three of the subunit interfaces suppresses channel activity. In contrast to this residue pair, the double mutant E235C/K393C produced a leak current that was prevented by reducing conditions and further increased by oxidative treatment, indicating that it is due to disulfide bond formation between E235C and K393C. Some of the oxidation-induced effects observed in this study were reversible in the presence of TCEP, whereas others were not. In the cases where TCEP had no effect, it is possible that the disulfide bonds were not accessible for the reducing reagent.

Conformational Changes of the Finger Loop and the Knuckle—The VCF experiments indicate that the distance between Trp-233 and labeled residues in the knuckle (K388C, Y389C, K392C) and the finger loop (Glu-235) increases upon acidification. The Trp-233 residue sits on top of the finger loop containing Glu-235 (Figs. 7A and 8). A rapid increase in distance between Trp-233 and labeled residues of the finger α 2 helix has previously been shown (14). The observation of a rapid Trp-233-dependent fluorescence increase of residues on different sides of the knuckle helix indicates that the knuckle

Author Contributions—K. G. and S. K. designed the study. K. G., G. B., and S. V. carried out the experiments. S. K. and K. G. wrote the manuscript. All authors participated in the analysis of the data and approved the final version of the manuscript.

Acknowledgments—We thank Omar Alijevic, Olivier Poirot, and Miguel van Bemmelen for comments on the manuscript, Sophie Roy for the construction of some mutants, and Cláudia Igutti Suenaga Lelli for some VCF measurements.

References

- Krishtal, O. A., and Pidoplichko, V. I. (1981) A receptor for protons in the membrane of sensory neurons may participate in nociception. *Neuroscience* **6**, 2599–2601
- Wemmie, J. A., Taugher, R. J., and Kreple, C. J. (2013) Acid-sensing ion channels in pain and disease. *Nat. Rev. Neurosci.* **14**, 461–471
- Kellenberger, S., and Schild, L. (2015) International Union of Basic and Clinical Pharmacology. XCI. Structure, function, and pharmacology of acid-sensing ion channels and the epithelial Na⁺ channel. *Pharmacol. Rev.* **67**, 1–35
- Wemmie, J. A., Askwith, C. C., Lamani, E., Cassell, M. D., Freeman, J. H., Jr., and Welsh, M. J. (2003) Acid-sensing ion channel 1 is localized in brain regions with high synaptic density and contributes to fear conditioning. *J. Neurosci.* **23**, 5496–5502
- Xiong, Z. G., Zhu, X. M., Chu, X. P., Minami, M., Hey, J., Wei, W. L., MacDonald, J. F., Wemmie, J. A., Price, M. P., Welsh, M. J., and Simon, R. P. (2004) Neuroprotection in ischemia: blocking calcium-permeable acid-sensing ion channels. *Cell* **118**, 687–698
- Jasti, J., Furukawa, H., Gonzales, E. B., and Gouaux, E. (2007) Structure of acid-sensing ion channel 1 at 1.9 Å resolution and low pH. *Nature* **449**, 316–323
- Bartoi, T., Augustinowski, K., Polleichtner, G., Gründer, S., and Ulbrich, M. H. (2014) Acid-sensing ion channel (ASIC) 1a/2a heteromers have a flexible 2:1/1:2 stoichiometry. *Proc. Natl. Acad. Sci. U.S.A.* **111**, 8281–8286
- Baconguis, I., Bohlen, C. J., Goehring, A., Julius, D., and Gouaux, E. (2014) X-ray structure of acid-sensing ion channel 1-snake toxin complex reveals open state of a Na⁺-selective channel. *Cell* **156**, 717–729
- Baconguis, I., and Gouaux, E. (2012) Structural plasticity and dynamic selectivity of acid-sensing ion channel-spider toxin complexes. *Nature* **489**, 400–405
- Gonzales, E. B., Kawate, T., and Gouaux, E. (2009) Pore architecture and ion sites in acid-sensing ion channels and P2X receptors. *Nature* **460**, 599–604
- Dawson, R. J., Benz, J., Stohler, P., Tetaz, T., Joseph, C., Huber, S., Schmid, G., Hügin, D., Pflimlin, P., Trube, G., Rudolph, M. G., Hennig, M., and Ruf, A. (2012) Structure of the acid-sensing ion channel 1 in complex with the gating modifier Psalmotoxin 1. *Nat. Commun.* **3**, 936
- Paukert, M., Chen, X., Polleichtner, G., Schindelin, H., and Gründer, S. (2008) Candidate amino acids involved in H⁺ gating of acid-sensing ion channel 1a. *J. Biol. Chem.* **283**, 572–581
- Liechti, L. A., Bernèche, S., Bargeton, B., Iwaszkiewicz, J., Roy, S., Michielin, O., and Kellenberger, S. (2010) A combined computational and functional approach identifies new residues involved in pH-dependent gating of ASIC1a. *J. Biol. Chem.* **285**, 16315–16329
- Bonifacio, G., Lelli, C. I., and Kellenberger, S. (2014) Protonation controls ASIC1a activity via coordinated movements in multiple domains. *J. Gen. Physiol.* **143**, 105–118
- Zha, X. M., Wang, R., Collier, D. M., Snyder, P. M., Wemmie, J. A., and Welsh, M. J. (2009) Oxidant regulated inter-subunit disulfide bond formation between ASIC1a subunits. *Proc. Natl. Acad. Sci. U.S.A.* **106**, 3573–3578
- García-Añoveros, J., Derfler, B., Neville-Golden, J., Hyman, B. T., and Corey, D. P. (1997) BNaC1 and BNaC2 constitute a new family of human neuronal sodium channels related to degenerins and epithelial sodium channels. *Proc. Natl. Acad. Sci. U.S.A.* **94**, 1459–1464
- Chen, X., and Gründer, S. (2007) Permeating protons contribute to tachyphylaxis of the acid-sensing ion channel (ASIC) 1a. *J. Physiol.* **579**, 657–670
- Vukicevic, M., Weder, G., Boillat, A., Boesch, A., and Kellenberger, S. (2006) Trypsin cleaves acid-sensing ion channel 1a in a domain that is critical for channel gating. *J. Biol. Chem.* **281**, 714–722
- Hille, B. (2001) *Ion Channels of Excitable Membranes*, 3rd Ed., pp. 441–470, Sinauer Associates, Sunderland
- Petterson, E. F., Goddard, T. D., Huang, C. C., Couch, G. S., Greenblatt, D. M., Meng, E. C., and Ferrin, T. E. (2004) UCSF Chimera: a visualization system for exploratory research and analysis. *J. Comput. Chem.* **25**, 1605–1612
- Zerangue, N., Schwappach, B., Jan, Y. N., and Jan, L. Y. (1999) A new ER trafficking signal regulates the subunit stoichiometry of plasma membrane K(ATP) channels. *Neuron* **22**, 537–548
- Li, T., Yang, Y., and Canessa, C. M. (2009) Interaction of the aromatics Tyr-72/Trp-288 in the interface of the extracellular and transmembrane domains is essential for proton gating of acid-sensing ion channels. *J. Biol. Chem.* **284**, 4689–4694
- Chu, X. P., Close, N., Saugstad, J. A., and Xiong, Z. G. (2006) ASIC1a-specific modulation of acid-sensing ion channels in mouse cortical neurons by redox reagents. *J. Neurosci.* **26**, 5329–5339
- Andrey, F., Tsintsadze, T., Volkova, T., Lozovaya, N., and Krishtal, O. (2005) Acid sensing ionic channels: modulation by redox reagents. *Biochim. Biophys. Acta* **1745**, 1–6
- Cho, J. H., and Askwith, C. C. (2007) Potentiation of acid-sensing ion channels by sulfhydryl compounds. *Am. J. Physiol. Cell Physiol.* **292**, C2161–C2174
- Lingueglia, E., de Weille, J. R., Bassilana, F., Heurteaux, C., Sakai, H., Waldmann, R., and Lazdunski, M. (1997) A modulatory subunit of acid sensing ion channels in brain and dorsal root ganglion cells. *J. Biol. Chem.* **272**, 29778–29783
- Kleyman, T. R., and Cragoe, E. J., Jr. (1988) Amiloride and its analogs as tools in the study of ion transport. *J. Membr. Biol.* **105**, 1–21
- Adams, C. M., Snyder, P. M., and Welsh, M. J. (1999) Paradoxical stimulation of a DEG/ENaC channel by amiloride. *J. Biol. Chem.* **274**, 15500–15504
- Alijevic, O., and Kellenberger, S. (2012) Subtype-specific modulation of acid-sensing ion channel (ASIC) function by 2-guanidine-4-methylquinazoline. *J. Biol. Chem.* **287**, 36059–36070
- Pantazis, A., and Olcese, R. (2012) Relative transmembrane segment rearrangements during BK channel activation resolved by structurally assigned fluorophore-quencher pairing. *J. Gen. Physiol.* **140**, 207–218
- Krauson, A. J., Rued, A. C., and Carattino, M. D. (2013) Independent contribution of extracellular proton binding sites to ASIC1a activation. *J. Biol. Chem.* **288**, 34375–34383
- Roy, S., Boiteux, C., Alijevic, O., Liang, C., Bernèche, S., and Kellenberger, S. (2013) Molecular determinants of desensitization in an ENaC/degenerin channel. *FASEB J.* **27**, 5034–5045